NURETH14-010

VALIDATION OF NEPTUNE CFD TWO PHASE FLOW MODELS USING THE OECD/NRC BFBT BENCHMARK DATABASE

J. Pérez, M. Böttcher, V. Sánchez,

Karlsruhe Institute of Technology (KIT), Institute for Neutron Physics and Reactor Technology (INR)
Hermann-von-Helmholtz-Platz 1, D-76344 Eggenstein-Leopoldshafen, GERMANY

jorge.perez@inr.fzk.de

Abstract

In this work the flow within a fuel assembly of a boiling water reactor was modeled using NEPTUNE-CFD. The most important parameters to define the flow like the incipient boiling condition, the heat flux partitioning and the heat transfer models are identified and tested against experimental data from BFBT bundle test. Different heat transfer models are applied for the water/steam interface. Additionally the heat conduction is solved for the insulator and cladding of the heater rods by coupling NEPTUNE-CFD with the SYRTHES package. The calculated average void fractions are in good agreement with the experimental data and the areas for future improvements are identified.

Introduction

One of the most important fields in nuclear power plant design analysis is the prediction of the thermo-hydraulic core behaviour. Recent advances have lead to a gradual improvement in the modelling and simulation of thermal hydraulic systems allowing a better assessment of the plant safety. The latest advances in the field of computational fluid dynamics allow to predict more accurately key thermal hydraulic parameters at different conditions and at different spatial scales. Computational Fluid Dynamic codes (CFD) can describe single phase flow phenomena with good accurate, while they need more improvements for the two phase flow boiling modelling. EDF (*Electricité de France*), CEA (*Commissariat à l'Energie Atomique*) sponsored by IRSN (*Institute de Radioprotection et de Sûreté Nucléaire*) and AREVA are developing a new CFD code for nuclear reactor applications called NEPTUNE-CFD. In the frame of the Nuclear Reactor Integrated Simulation Project (NURISP) this code is being enhanced and validated using different types of experiments. In this paper, the investigations performed to validate the two phase flow models of NEPTUNE-CFD under transient conditions using the data of the BFBT test are presented and discussed in detail.

1. Description of the BFBT experiment

The OECD/NRC benchmark NUPEC BWR Full-Size Fine-Mesh Bundle Test (BFBT) [1], provides a suitable database for validation and improvement of subchannel and CFD two phase flow models. The BFBT benchmark is composed of two different parts, the void distribution benchmark (Phase I) and the critical power benchmark (Phase II). An exercise from Phase I was selected for the validation of NEPTUNE-CFD. The transient tests performed in the frame of this benchmark represent the thermal hydraulic conditions that may be encountered during a postulated BWR turbine trip transient without bypass. From this postulated turbine trip transient

important thermal hydraulic parameters were derived for the test such as the evolution of the pressure, total bundle power, mass flow, radial and axial power profile which serves as initial and boundary conditions for the CFD simulations. Many parameters were measured during the tests which will be used for comparisons with the code predictions.

1.1 Test section and experiment conditions

The test section of the experiment is a full sized 8x8 BWR fuel assembly with sixty electrically heated rods and one water channel. The heated section is 3708 mm long and the heaters are surrounded by an insulator (boron nitride) and by the cladding (Inconel 600). A X-ray densitometer is used to measure the averaged void fraction at different axial levels.

In case of a turbine trip transient, a pressure wave propagates from the steam line to the core due to the fast closure of the turbine stop valves and because the bypass valves remain close. As a consequence, the void in the core collapses improving the moderation of neutrons and hence leading to a sudden power increase. Due to the power increase, the fuel temperature increases too. Due to the increase absorption of neutrons in U-238 (Doppler Effect) the power increase is stopped. Depending of the conditions of the main recirculation pumps, the total power will reduces and it will stabilizes at a lower power level. As long the recirculation flow is low, Figure. 2, the power remains low, and it will increase if the mass flow rate increases due to the improved moderation. In Figure. 1, Figure. 2 and Figure. 4 the evolution of the outlet pressure, the mass flow rate and the power during the first 60 seconds of the transient time is given. The experiment is performed with a constant axial power shape. The radial power shape is described by Figure. 6. The water inlet temperature remains constant at 552 K during the experiment.

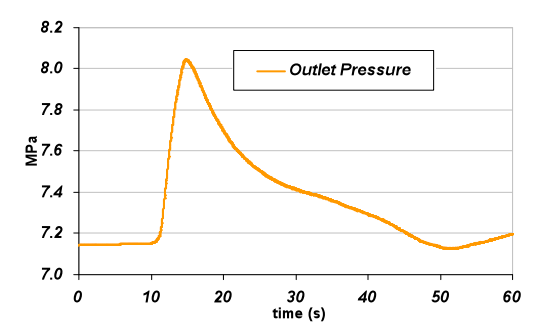


Figure. 1. Pressure evolution

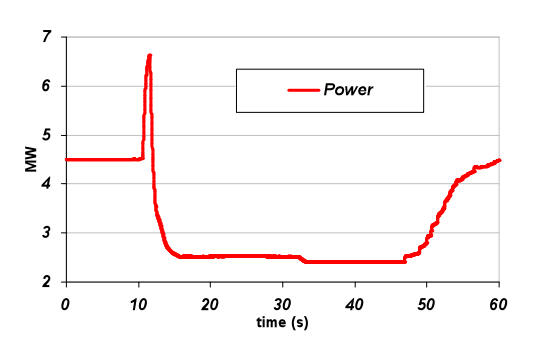


Figure. 4. Power evolution

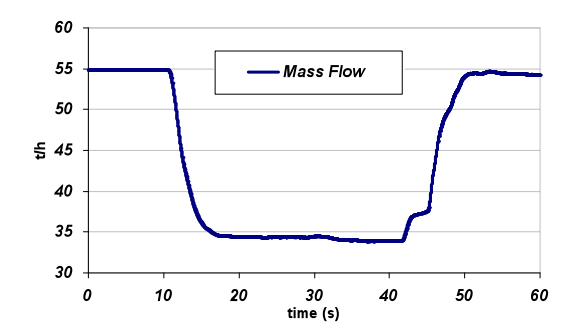


Figure. 2. Mass flow rate evolution

1.15	1.30	1.15	1.30	1.30	1.15	1.30	1.15
1.30	0.45	0.89	0.89	0.89	0.45	1.15	1.30
1.15	0.89	0.89	0.89	0.89	0.89	0.45	1.15
1.30	0.89	0.89			0.89	0.89	1.15
1.30	0.89	0.89			0.89	0.89	1.15
1.15	0.45	0.89	0.89	0.89	0.89	0.45	1.15
1.30	1.15	0.45	0.89	0.89	0.45	1.15	1.30
1.15	1.30	1.15	1.15	1.15	1.15	1.30	1.15

Figure. 6. Radial power shape coefficients

2. Short description of relevant two phase flow models in Neptune CFD

The two phase flow water-steam-mixture is described by an Euler-Euler approach with liquid as continuous and steam as dispersed phase. A single pressure field is shared by all phases. Momentum, energy and continuity conservation equations are solved for each phase. A k-ɛ turbulence model for the liquid phase is used with standard wall function. Laminar flow is considered for the dispersed phase. The libraries for the liquid properties are provided by the system code CATHARE, furthermore steam close to saturation conditions is assumed. For heat transfer through the gas/liquid interface a thermal phase change model is applied. The heaters are modelled in terms of a heat flux boundary condition. At the inlet, a mass flow rate is set and the pressure is imposed at the outlet. The phenomena which will be described in the frame of this investigation are: the incipient boiling condition, the wall heat partitioning, the heat exchange between phases and the bubble diameter.

2.1 Incipient boiling condition

The incipient boiling point is based on Hsu's criterion [2]. According to this criterion a bubble will grow from a vapour embryo in a cavity if the liquid temperature surrounding the cavity is at least equal to saturation. The wall superheating at boiling incipience can be calculated from the wall heat flux ϕ_{wall} , in Eq. (1). If the wall temperature reaches the critical value, the cavities of radius equal to r_{cl} are activated. If the temperature still increases, smaller cavities are activated, too. If the biggest radius (r_{cmax}) of the largest cavity available on the surface is smaller than the r_{cl} , the required wall superheating is higher, see Eq. (2).

$$T_{wall} - T_{sat} = T_{crit_1} = \left(\frac{8 \cdot \sigma \cdot T_{sat}}{H_{lat} \cdot \rho_{lsat}} \cdot \frac{\varphi_{wall}}{\lambda_l}\right)^{1/2} \qquad r_{cl} = \frac{\lambda_l \cdot T_{crit_1}}{2 \cdot \varphi_{wall}}$$
(1)

$$T_{wall} - T_{sat} = T_{crit_2} = \frac{\varphi_{wall}}{\lambda_l} \cdot r_{c \max} + \frac{2 \cdot \sigma \cdot T_{sat}}{H_{lat} \rho_{l sat}} \cdot \frac{1}{r_{c \max}}, \tag{2}$$

where T_{sat} is the saturation temperature, H_{lat} the latent enthalpy, λ_l the thermal conductivity of the liquid, σ the surface tension and ρ_l the liquid density.

2.2 Boiling heat flux

The wall boiling model used by NEPTUNE-CFD is an extension of the *Kurul* and *Podowski* model [3] that describes three fluxes due to convection, quenching and evaporation. In order to formulate each one of the 3 fluxes, it is necessary to specify the area of the wall occupied by bubbles (A_Q) , and by the liquid phase (A_C) . Those areas must verify: $A_Q + A_C = 1$. The area influenced by bubbles is a function of the bubble departure diameter D_d and the active site density n, Eq. (3).

$$A_{Q} = \min\left(1, \pi \cdot D_{d}^{2} \cdot \frac{n}{4}\right) \qquad n = \left[210 \cdot \left(T_{wall} - T_{sat}\right)\right]^{.8} \qquad D_{d} = 2.42 \cdot 10^{-5} \cdot P^{0.709} \cdot \frac{a}{\sqrt{b \cdot \beta}}$$
(3)

The coefficients from the active site density formula were correlated by [3]. The formulation for a, b and β coefficients from the bubble departure diameter (D_d) are:

$$a = \frac{\left(T_{wall} - T_{sat}\right) \cdot \lambda_{s}}{2 \cdot \rho_{g} \cdot H_{lat} \sqrt{\pi \cdot \left(\frac{\lambda_{l}}{\rho_{l} \cdot C_{pl}}\right)}} \qquad b = \frac{\left(T_{wall} - T_{\delta}\right)}{2 \cdot \left(1 - \frac{\rho_{g}}{\rho_{l}}\right)}$$

$$(4)$$

$$\beta = \begin{cases} \left(\frac{V_{\delta}}{V_0}\right)^{0.47} & \text{if } V_{\delta} > V_0 \\ 1 & \text{if } V_{\delta} < V_0 \end{cases} \qquad V_0 = 0.61 \,\text{m/s}$$
 (5)

The index (s) refers to the solid wall. The index (δ) refers to a point in the fluid turbulent boundary layer. These correlations were developed for subcooled water flow by H.C.Unal [4]. At the area of the wall unaffected by the presence of bubbles, the convective heat flux is given by:

$$\varphi_C = A_C \cdot q \cdot \left(T_{wall} - T_\delta\right) \,, \tag{6}$$

where q represents the heat transfer within the thermal boundary layer. The quenching heat flux is defined in Eq. (7). As a consequence of the bubble departure, the wall is brought in contact with cold water periodically.

$$\varphi_{Q} = A_{Q} \cdot t_{Q} \cdot f \cdot \frac{2 \cdot \lambda_{l} \cdot (T_{wall} - T_{\delta})}{\sqrt{\pi \cdot \omega_{l} \cdot t_{Q}}}$$

$$(7)$$

In Eq. (7), ω_l is the thermal liquid diffusivity, f is the bubble departure frequency, and $t_Q = 1/f_Q$ is the time fraction during quenching. The evaporation heat flux is described in Eq. (8) and it is proportional to the volume of the bubble V_b :

$$\varphi_E = V_b \cdot f \cdot \rho_g \left(H_g - H_l \right) \qquad V_b = \frac{\pi \cdot D_d^3}{6}, \tag{8}$$

where H_g and H_l are the enthalpy jumps related to the mass transfer. NEPTUNE-CFD makes a generalization of the heat flux decomposition model and adds a new heat flux [5]. The fourth flux is transmitted directly from the wall into the steam phase, Eq.(9)

$$\varphi_{wall} = \left(f_{\alpha_1} \cdot \varphi_1 - \Gamma^{nuc} H_I \right)_{(wall \to I)} + \left(f_{\alpha_2} \varphi_2 + \Gamma^{nuc} H_g \right)_{(wall \to g)} \qquad \Gamma^{nuc}_{(wall \to g)} = -\Gamma^{nuc}_{(wall \to I)}$$
(9)

Where φ is the heat flux and Γ^{nuc} is the mass transfer by wall nucleation. The function $f_{\alpha 1}$ depends on the void fraction α_1 , $f_{\alpha 2}$ is defined as follows: $f_{\alpha 2} = 1 - f_{\alpha 1}$. In NEPTUNE-CFD, a critical value for the liquid void fraction is selected to determinate the wall heat flux decomposition. Depending on the value of α_1 the definition for $f_{\alpha 1}$ is explained below.

$$\alpha_{1} > \alpha_{crit} \rightarrow f_{\alpha 1} = 1 - \frac{1}{2} \cdot e^{-20(\alpha_{1} - \alpha_{1,crit})} \qquad \alpha_{1} < \alpha_{crit} \rightarrow f_{\alpha 1} = \frac{1}{2} \cdot \left(\frac{\alpha_{1}}{\alpha_{crit}}\right)^{20 \cdot \alpha_{crit}}$$
(10)

The value for the α_{crit} is 0.2. To select the characteristics of the liquid for the wall boiling model, it is recommended not to take the information from the wall closest cell due to the mesh dependency. At this location high temperature and void fraction gradients are expected. *Egorov* and *Menter* [6] restored the mesh independence by using the logarithmic law of the wall function to estimate the liquid temperature at the fixed value of $y^+ = 250$ which is used in NEPTUNE-CFD.

2.3 Interfacial area concentration

Following W. Yao and C. Morel [7], the specific interfacial area equation (IAE) is calculated as:

$$\frac{\partial A_i}{\partial t} + div \cdot \left(A_i \cdot \vec{V}_i \right) = \frac{2}{3} \cdot \frac{A_i}{\alpha \rho_g} \left(\Gamma_{g,i} - \alpha \frac{d\rho_g}{dt} \right) + 12 \cdot \pi \cdot \left(\frac{\alpha}{A_i} \right)^2 \cdot \left[\phi_n^{CO} + \phi_n^{BK} \right] + \pi \cdot d_{nuc}^2 \cdot \phi_n^{NUC}. \tag{11}$$

The bubble diameter is calculated in this equation with some restrictions, the minimum bubble size has to be set by the user. By assuming spherical bubbles, the equation is providing a single bubble size given by d_s . The Sauter mean diameter and the bubble number density (n) are related to the IAE and the void fraction by the following relations:

$$d_s = \frac{6\alpha}{A_i} \qquad n = \frac{1}{36 \cdot \pi} \cdot \frac{A_i^3}{\alpha^2}, \tag{12}$$

where A_i is the interfacial area concentration. The nucleation term is calculated from the wall nucleation model. Breakup and coalescence models are proposed by *Yao* and *C.Morel* [8].

2.4 Interface steam-water heat transfers

If the mechanical terms are neglected in comparison to the thermal effects in the averaged form of energy jump condition, the interfacial transfer term of mass Γ_k , and the interfacial transfer term of heat S'_{ki} must verify:

$$\sum_{k} \left(\Gamma_{k} \cdot H_{ki} + S_{ki}' \cdot A_{i} \right) \approx 0 \tag{13}$$

 H_{ki} is the jump of enthalpy associated with mass transfer from phase k to the interface. This relation together with the mass jump condition: $\Gamma_l = -\Gamma_g$, allows to compute:

$$\Gamma_{l} = -\Gamma_{g} = \frac{S_{li}^{'} + S_{gi}^{'}}{H_{\sigma i} - H_{li}} \cdot A_{i}$$

$$\tag{14}$$

S'_{li} is the heat transfer term from the liquid to the interface, and S'_{gi} is the heat transfer term from the gas phase to the interface. The model chosen for the heat transfer term of the liquid phase is based on Ranz-Marshall approach. The heat transfer coefficient is given below according to [9].

$$S_{li} = q_{li} \cdot (T_{sat} - T_l) \qquad q_{li} = \frac{\lambda_1}{d_s} \cdot Nu$$
 (15)

Depending on the Jakob number given by Eq. (16), there are two possible scenarios, condensation (Ja \leq 0) or evaporation (Ja \geq 0).

$$Ja = \frac{\rho_l \cdot C_{pl} \cdot (T_l - T_{sat})}{\rho_{\sigma} \cdot L} \tag{16}$$

The thermal capacity of the liquid is C_{pl} , and L is the latent heat of vaporization. In case of condensation, the Nusselt number is given by Eq. (17).

$$Nu = 2 + 0.6 \cdot \text{Re}^{1/2} \, \text{Pr}^{1/3}$$
 $\text{Re} = \frac{d_s \cdot |V_g - V_l|}{\mu_l}$ $\text{Pr} = \frac{\mu_1}{\omega_l}$ (17)

where μ_l is the liquid kinematic viscosity. In case of evaporation the Nusselt number is defined as follows:

$$Nu = \max(Nu_1, Nu_2, Nu_3)$$
 $Nu_1 = \sqrt{\frac{4 \cdot Pe}{\pi}}$ $Nu_2 = \frac{12}{\pi} \cdot Ja$ $Nu_3 = 2$ (18)

Where Pe is the Péclet number and it is defined as follows:

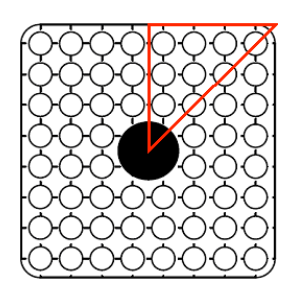
$$Pe = \text{Re} \cdot \text{Pr} = \frac{d_s |V_g - V_l|}{\omega_l} \quad . \tag{19}$$

A constant time scale for returning to saturation was used for the steam to solve the steam-interface heat transfers. It is assumed that the steam remains at saturation temperature by rapid evaporation/condensation. The model for the steam interface is described below:

$$S_{gi} = \alpha_g \frac{\rho_g \cdot C_{pg}}{\tau} \left(T_{sat} - T_g \right) \tag{20}$$

3. Numerical simulation

Three different heat transfers terms are tested: the Astrid model by J.Laviéville and O. Simonin [10]. The Ranz-marshall model formulated in the previous chapter, and the "Flashing model" that takes into account a delayed condensation, T.Masciaszek et. al. [11]. The time step is adaptative depending on Courant number, the range of the steps is from 1ms to 3ms. The convergence criteria for the residuals remains very severe as it applies to a maximum value over the whole domain of 10⁻⁵. The Due to the long calculation time required, preliminary simulations were performed on a single subchannel test case. The simulations are conditioned by the large amount of void present at the domain. Numerical simulations find convergence problems in very refine meshes with boiling flow, especially in the water and steam temperature close to the heated wall region. If the void concentration at the wall region is high, then the heat flux tends to overheat the steam. This situation can be mitigated by increasing the cell size. More information about nodalization sensitivity analyses on boiling flow within subchannels with NEPTUNE CFD is available by J.Perez and M.Böttcher [12]. The preliminary simulations provide information about the proper nodalization geometry for this exercise. The nearest wall heated region cell has a constant width of 0.3 mm. The mesh is composed by 135 axial levels and 12 cross cells in each subchannel and it has 211928 cells. The maximum y values are located close to the outlet, they oscillate between 300 and 400, depending on the transient conditions. Taking into account the axial symmetry of the fuel assembly, only a 45° part of the fluid domain is modeled (Fig. 5).



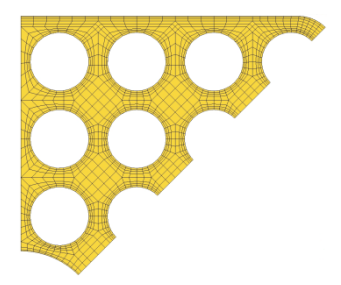


Fig. 8. Assembly type No.4 (high burn-up) and nodalization geometry.

For the initialization of the simulation the power is increased gradually from 0 to nominal value, which is reached after 6 seconds. The drag and non drag forces: lift, added mass and turbulent dispersion force are computed for the simulation. Since the IAE requires a minimum bubble size, two different values are chosen: 0.15 and 1 mm. Previous studies on the IAE implemented by NEPTUNE CDF, *J.Perez et. al* [13], demonstrated that minimum bubble sizes larger than 0.2 mm can slightly modify the void prediction compared with smaller diameters. In this case one value above and one value below 0.2 mm are selected to check the simulation sensitivity to this diameter. As boundary conditions, experimental data is used. At the inlet the mass flow rate (Fig.2) with a constant temperature of 552 K is assumed, while at the outlet an absolute pressure (see Fig.1) is specified. Two options are used for modeling the pin heat release. The first option is to locate the flux at the rod wall of the fluid domain, the second option is to model the clad and insulator and place the heat flux into the inner diameter insulator surface. Since NEPTUNE-CFD is not able to solve a conjugate heat transfer through solid by itself, it has to be coupled with the thermal tool SYRTHES [14]. Table 1 summarizes the simulations performed. The averaged void fraction evolution for the cross sectional area of the fuel assembly is calculated for three axial

levels, (0.67m, 1.72 m and 2.7 m) from the beginning of the heated section. Figure 6 shows the location of the measured sections. At the same figure the local void fraction distribution is shown for different time steps of the transient: at second 7, at second 11.45, during the maximum void concentration, at second 20, 30 and at second 50, where the combination of power and mass flow decreases the void to the minimum values of the experiment.

Run Number	Min Bubble Size (mm)	H.T. Model water/steam	SYRTHES
T1	0.15	"Ranz-Marshall"/sat.	N
T2	0.15	"Flashing"/sat.	N
T3	0.15	"Ranz-Marshall"/sat.	Y
T4	1	"Ranz-Marshall"/sat.	N
T5	0.15	"Astrid"/sat.	N

Table 1. Performed simulations (test 4102-001-009)

4. Comparison of predictions with data

The comparison between the predicted evolution of the void average and experimental data for the different axial levels is shown by Figure 7, 8 and 9. In Figure 10, the local temperature of the water and steam is shown together with the saturation temperature. Those temperatures are taken from one point near the wall region of the rod 7 at the end of the heated section of the simulation T3, where the temperatures are expected to be the highest of the domain.

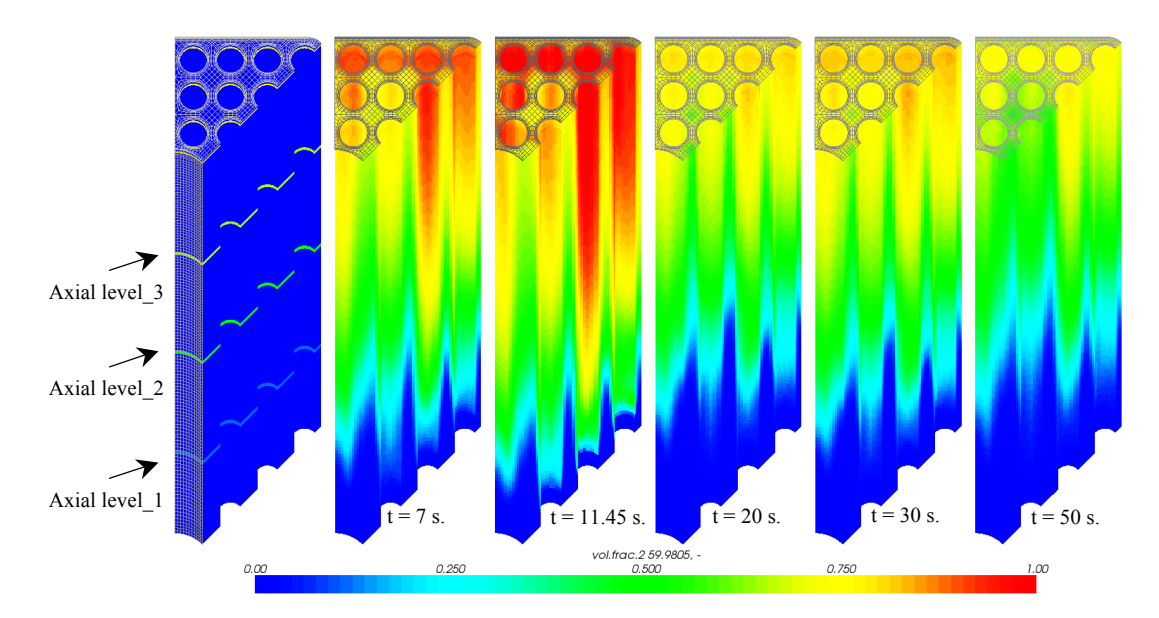


Fig. 9. Location of the axial levels and local void distribution for four different time steps.

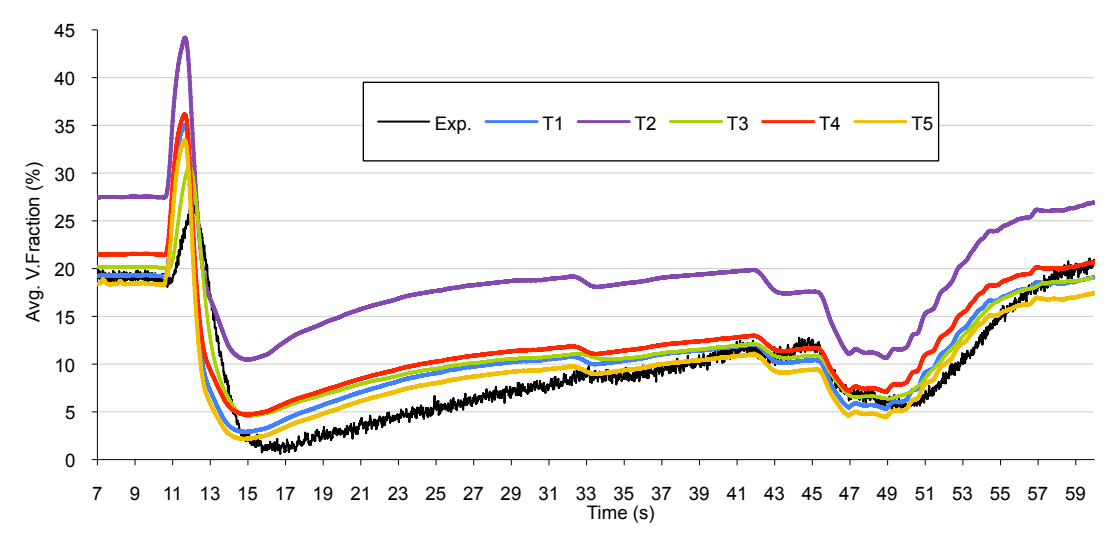


Fig. 10. Axial level_1 (0.67m): Averaged void fraction evolution.

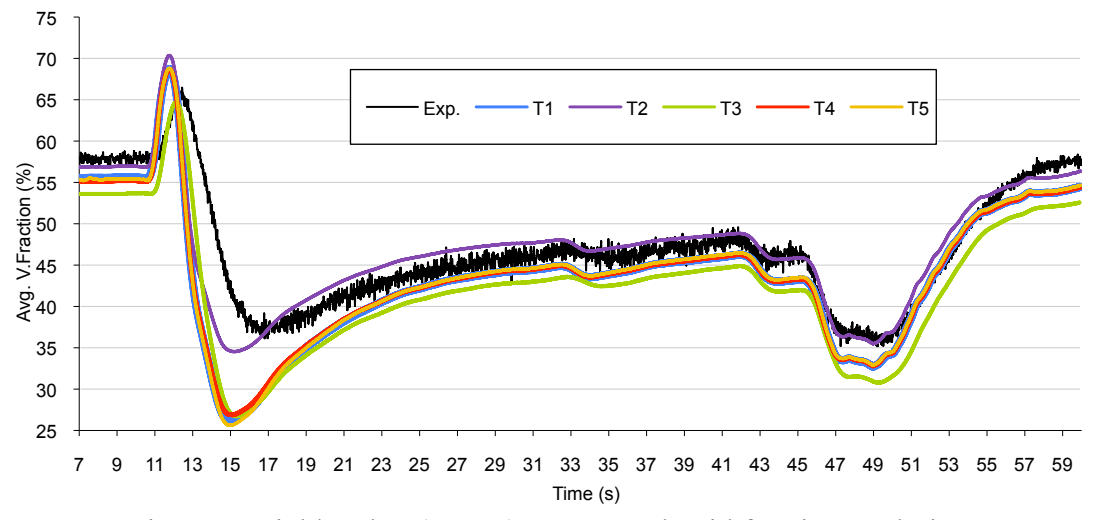


Fig. 11. Axial level 2 (1.72m): Averaged void fraction evolution.

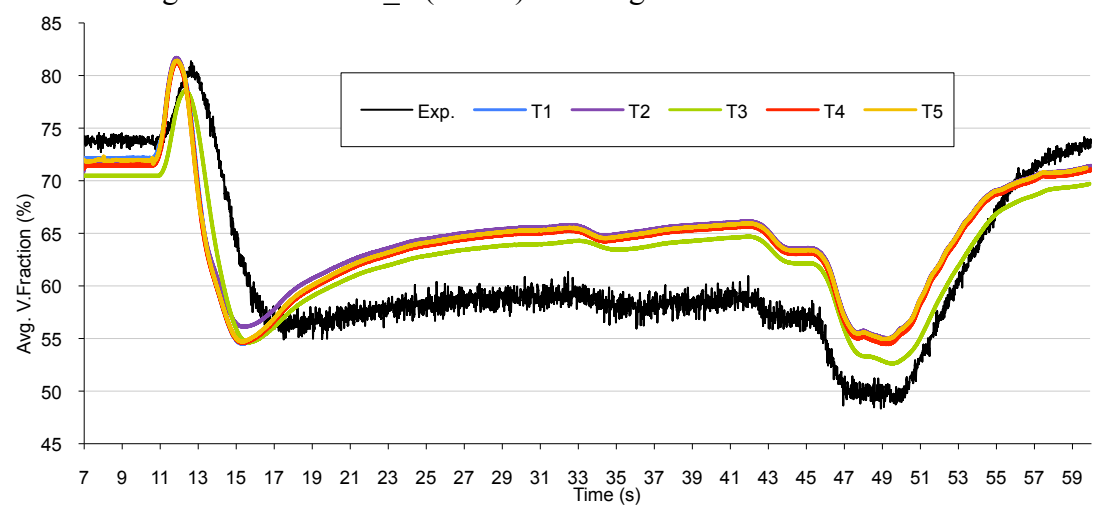


Fig. 12. Axial level_3 (2.7 m): Averaged void fraction evolution.

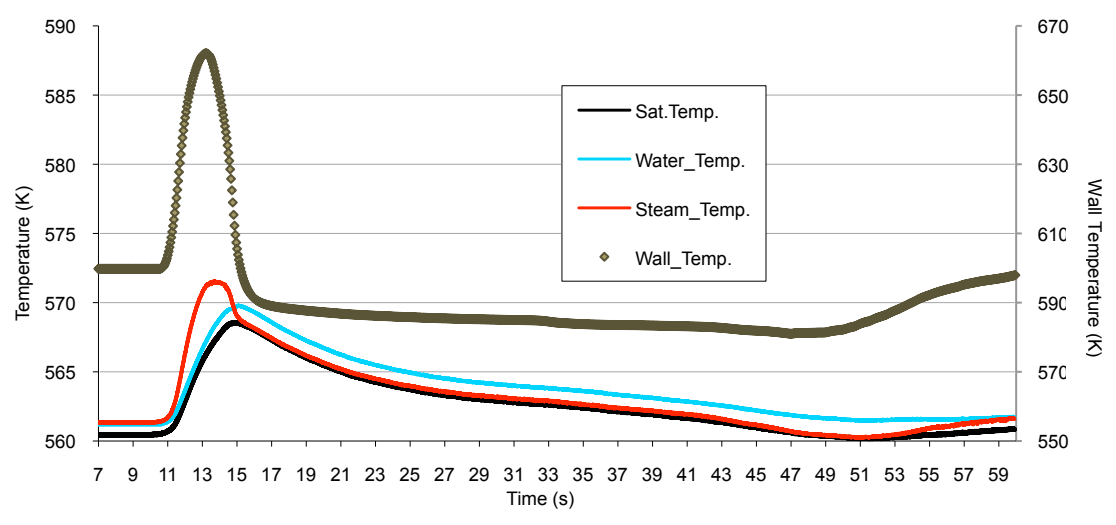


Fig. 13. Evolution of the saturation, steam and liquid temperature.

Up to 10 seconds under constant boundary conditions a good agreement with experimental data is obtained, especially the run T1 at the lower measurement location. Only run T2 is clearly overpredicting the void for the whole transient (Figure.7), because this heat transfer model was not developed for bubbly flow. Further downstreams at the axial levels 2 and 3 all runs are slightly underpredicting the void. At second 10.5 there is a power peak plus a flow decrease that produces a large amount of steam in the domain. At that moment all runs are over predicting the void for the first axial level, while for the axial levels 2 and 3 the simulations are on the range of the experimental data. The simulated void evolution during the power peak unveils the "fast" steam generation produced in the domain. While the experimental data has a gradual increase, the calculated void has a violent increase as soon as the power peak appears. The maximum void fraction calculated during the simulations fits in time with the maximum power peak, and the maximum void measured during the experiment has a time delay from 0.5 to 1 second (depending on the location). Only run T3 is producing a little delay in the steam generation, in this simulation the heat flux is defined in SYRTHES and the insulator and cladding effect is taken into account. The calculated void condensation during the power decrease is on the range of the data for runs T1, T3, T4 and T5 at the first axial level. At the axial location 2 (Fig. 9) the condensation ratio is over estimated and the averaged void decreases to the 25 % while the experimental void measured remains at 37 %. From second 17 the power and mass flow are stabilized and the moderate void fraction increase is related with the pressure decrease. At second 33 there is a small power drop with its correspondent void decrease. From second 42 the mass flow starts recovering up to nominal values, leading to void decrease. At second 47 the power start increasing again following the void fraction, up to initial conditions. During this period, after the power peak and the stabilization of the power and mass flow, the void prediction of the simulations T1, T3 and T4 shows a good agreement with experimental data for the first two location, and an over estimation for the third axial level.

Concerning the calculation with the "Flashing" liquid-interface heat transfer term, the difference with the Astrid or the Ranz-marshall model is that it is overestimating the void for the lower measure location (Fig. 7). This model has a good agreement especially during the condensation process after the power peak, at the axial location 2 (Fig. 8). For the third location (Fig. 9) there are no significant differences between the heat transfer models.

The differences between the two minimum bubble diameters (T1 and T4) are only appreciable at axial level 1 (Fig. 7), where the regime is bubbly flow and the main phenomena is subcooled boiling. At further downstream locations, the results are similar for the whole transient and the selection of the minimum diameter is less important. Deeper investigations on the minimum bubble size with NEPTUNE-CFD in subchannels are available in [13].

The coupling of NEPTUNE-CFD with SYRTHES lead to significant improvement due to the accurate steam temperature calculation, see Fig.10. In simulation T3, during the power peak the steam temperature remains as maximum at 3 degrees over saturation, while in other simulation without solving the thermal wall problem this temperature can reach locally hundreds of degrees over saturation, which is not physically correct. This is due to the fact that the heat flux is released directly into the fluid domain. On the other hand if the flux is defined at the insulator, the water and steam temperatures are calculated in a better way since SYRTHES is providing the wall temperature. Thus, the heat flux at the interface solid-fluid is calculated according to Eq.(21), with the wall and fluid temperature (T_w, T_f) and a heat transfer coefficient.

$$q_{w} = \frac{\rho \cdot c_{p} \cdot u^{*}}{T^{+}} \cdot \left(T_{w} - T_{f}\right) \tag{11}$$

Hence the heat flux from the wall to the steam phase is regulated avoiding excessive overheating. The wall temperature increases at those locations with high void fraction. In Fig.10, the local temperature jump between the wall and the liquid oscillate from 20 to 30 degrees during the transient, but at the power peak this difference rises up to 90 degrees.

5. Summary and conclusions

This work is a contribution to validate the two phase flow conditions that may occur during a turbine trip transient test. A wide range of averaged void fraction is calculated, from single phase flow to values up to 83 % void fraction. Different heat transfer models available in NEPTUNE-CFD were applied and compared. The coupling NEPTUNE-CFD with SYRTHES is used in this work and its capabilities are tested. The different location definitions of the heat flux as a boundary condition has a real effect on the simulation. The code is reproducing reasonably well the experimental data. The improvement area is located mainly at the rapid condensation modeling, where the code is underestimating the void fraction. The Flashing heat transfer term is describing this situation properly, but only for a range of void in between 35 % - 65 % (Fig. 8), for lower void fraction the model is overestimating the experimental data (Fig. 7). This over estimation is not only an issue of the heat transfer modeling, the assumption of a single bubble size per cell has also influence on the condensation. If all the bubbles have locally the same size they will condense at the same speed and their diameter will decrease accordingly. This can lead to an under estimation of the main bubble diameter. A multi size model would help by providing a more gradual condensation due to the local presence of different bubble diameters.

6. References

- [1] K. Ivanov, A. Hotta, E. Sartori. "OECD-NEA/US-NRC Benchmark based on NUPEC BWR Full-size Fine-mesh Bundle Tests (BFBT)."
- [2] Y.Y.Hsu. "On the size range of acting nucleation cavities on a heating surface" *Journal of heat Transfer*, No84, pp 207-216, 1962.
- [3] N.Kurul, M.Z.Podowski. "Multidimensional effects is forced convection subcooled boiling" Conference on heat and mass transfer, Jerusalem, 1991.
- [4] H.C.Unal. "Maximun bubble diameter, maximum bubble growth time and bubble growth rate during subcooled nucleate flow boiling of water up to 17.7Mw/m2", *International journal Mass Transfer*, No 19.pp.643-649,1976.
- [5] Lavieville J., Quemerais E., Mimouni S., Boucker M., Mechitoua N. "Neptune CFD V1.0 Theory manual."
- [6] A.Burns, Y.Egorov, F.Menter. "Experimental Implementation of the RPI wall boiling model CFX-11", Ansys CFX Germany, April 2004.
- [7] W.Yao, C.Morel. "Volumetric interfacial area prediction in upward bubbly two-phase flow", *International Journal of heat and mass transfer* Vol.47 307-328,2004W.
- [8] W.Yao, C.Morel. "Prediction of parameters distribution of upward boiling two-phase flow with two fluid models", <u>ICONE</u> 10-22463.
- [9] S. Mimouni, F Archambeau, M.Boucker, J.Lavieville, C.morel. "A second order turbulence model based on a Reynols stress approach for two phase flow boiling flow. Part 1. Application to the ASU-Annular channel case", *Internal Journal Of Heat and Mass Transfer* 47(2004) 307-328.
- [10] J.Laviéville and O. Simonin. "Equations et modèles diphasiques du code Astrid 3.4 et du code saturne polyphasique", Technical Report HE-44/99/041A, EDF R&D,1999
- [11] T. Masciaszek, J.C. Micaelli, D. Bestion, "Modélisation de l'autovaporisation dans le cadre d'un modèle à deux fluides", La Houille blanche N°2-1988
- [12] J.Perez, M.Böttcher. "Progress report on two phase flow simulations in a subchannel with NEPTUNE 1.0.7" Nuclear Reactor Integrated Simulation Project. NURISP-D2.2.3.19.a.
- [13] J.Perez, M.Böttcher, V.Sanchez. "Validation of NEPTUNE-CFD two phase flow models using PSBT experiments" KTG-2011 (German Nuclear Society)
- [14] I.Rupp, C.Péniguel. "SYRTHES 3.4 User Manual" EDF R&D 2008

The 14^{th} International Topical Meeting on Nuclear Reactor Thermalhydraulics, NURETH-14 Toronto, Ontario, Canada, September 25-30, 2011